

Photoexcitation of a polarization-inverted domain from the charge-ordered ferroelectric ground state of $(\text{TMTTF})_2\text{PF}_6$

T. Yamaguchi,¹ K. Asada,² H. Yamakawa,² T. Miyamoto,²
K. Iwano,³ T. Nakamura,⁴ N. Kida,² and H. Okamoto^{2,5}

¹*Institute of Materials Structure Science,
High Energy Accelerator Research Organization (KEK),
1-1 Oho, Tsukuba 305-0801, Japan*

²*Department of Advanced Materials Science, The University of Tokyo,
5-1-5 Kashiwa-no-ha, Chiba 277-8561, Japan*

³*Graduate University for Advanced Studies,
Institute of Materials Structure Science,
High Energy Accelerator Research Organization (KEK),
1-1 Oho, Tsukuba 305-0801, Japan*

⁴*Institute for Molecular Science, Myodaiji, Okazaki, 444-8585, Japan*

⁵*AIST-UTokyo Advanced Operando-Measurement Technology Open Innovation Laboratory,
National Institute of Advanced Industrial Science and Technology, Chiba 277-8568, Japan*

(Dated: March 17, 2022)

Abstract

We theoretically revealed that a weak photoexcitation achieves the electric polarization-inversion with approximately 18% of all the charges, which was interpreted as a superimposition of multi-exciton states, from the charge-ordered ferroelectric ground state of $(\text{TMTTF})_2\text{PF}_6$ at absolute zero temperature. Regarding a relative change of electric polarization ($\Delta P/P$), the photoexcitation corresponds to 36%, which is much larger than $\Delta P/P$ of other typical organic materials. The value of $\Delta P/P \sim 36\%$ can be enlarged by a strong photoexcitation. This fact is useful not only for applications of this material and other analogous materials in optical devices but also for researches toward controlling electric polarizations by light, which is one of the recent attracting issues on photoinduced phase transition phenomena. The photoexcitation of $\Delta P/P \sim 36\%$ corresponds to the single peak of the optical conductivity in the low-energy region, which was also observed at 10 K. Theoretical calculations are based on a quarter-filled one-dimensional effective model with appropriate parameters and 50 unit cells.

PACS numbers: 71.30.+h, 71.35.Lk, 78.20.Bh

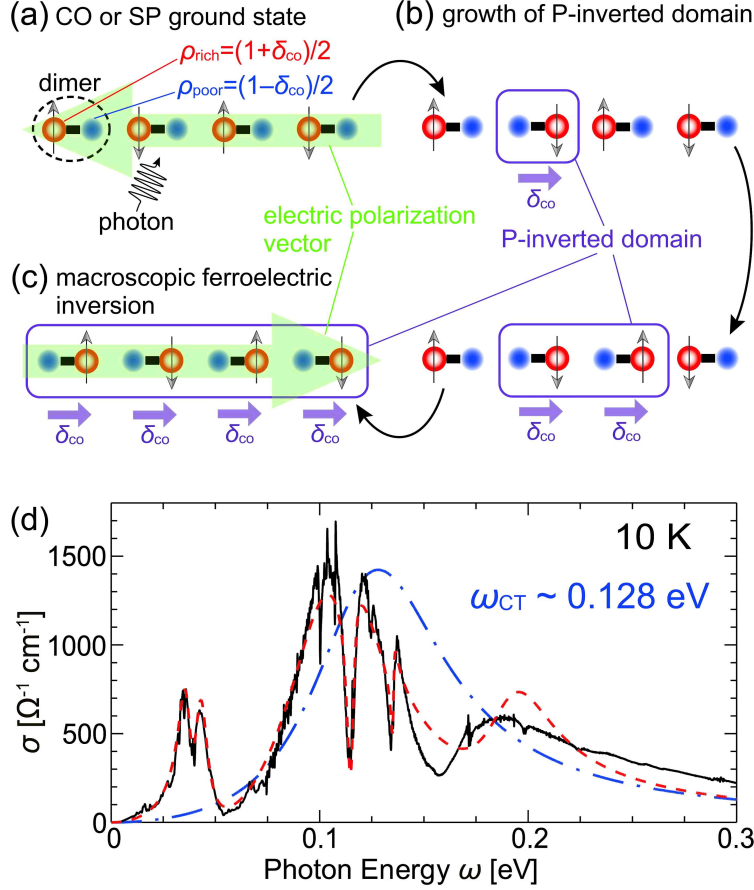


FIG. 1. (a)–(c) Schematics of the CO or SP ground state and photoexcited states of $(\text{TMTTF})_2\text{PF}_6$. The circle and up (down) arrows on the circles represent a molecular orbital of a TMTTF molecule and up (down) spins, respectively. (d) Optical conductivity spectrum of $(\text{TMTTF})_2\text{PF}_6$ with the electric field polarized parallel to the a -axis at 10 K (solid line) and the fitting curve (dashed line). The chained line shows the calculated spectrum with resonant energy 0.128 eV.

I. INTRODUCTION

Studies on controlling the purely electronic phase transitions occurring immediately after a photoexcitation from the ground state of matter have been attracting attention because such photoinduced phase transitions (PIPTs) regulate the macroscopic properties of matter on the ultrafast time scale [1, 2]. Once such electronic PIPTs are applied to organic ferroelectric materials, the electric polarization can be tuned in the regime of femtoseconds. Because of notable properties such as mechanical flexibility, disposability, and inexpensiveness, organic materials are increasingly being applied to electronic and optical devices. In this

regard, flexible tuning of a light-induced electric polarization in the order of femtoseconds is one of the most attracting challenge in the field of PIPTs, recently.

So far, as one of the light sources to easily create and control such devices, visible-light (light) is actually most convenient. In this regard, PIPTs induced by light has actively been studied. For instance, a light-induced ultrafast insulator–metal transition has been observed in a quasi-two-dimensional molecular solid, α -(BEDT-TTF) $_2$ I $_3$ (BEDT-TTF = bis(ethylenedithiolo)tetrathiafulvalene) [3]. Because the material undergoes ferroelectric polarization in the charge-ordered (CO) ground state [4, 5], this transition is regarded as a photoinduced disappearance of the polarization. A photoexcitation of a non-polarized state from a ferroelectric polarized ground state has been reported for a quasi-one-dimensional (1D) molecular solid, TTF-CA (tetrathiafulvalene-chloranil) [6]. Very recently, a photoinduced polarization suppression was observed in croconic acid and it was regarded as a light-induced polarization inversion of protons [7]. However, at present, we are not aware of any experimental achievement regarding a light-induced electronic ferroelectric inversion.

(TMTTF) $_2$ XF $_6$ (TMTTF = (tetramethyltetrathiafulvalene), X =P, As, Sb, Ta) is known as one of the quasi-1D quarter-filled organic conductors and it has rich physical phases [8–16]. In particular, the bulk electronic ferroelectricity of (TMTTF) $_2$ PF $_6$ caused by finite charge disproportion δ_{co} has been experimentally depicted [17–21] in both a CO phase and spin-Peierls (SP) phase. According to Ref. [9], the CO and SP phase of (TMTTF) $_2$ PF $_6$ have been achieved below 67 K and 19 K, respectively. In our study, representing ρ_{rich} (ρ_{poor}) as the rich (poor) value of the charge of the two closest TMTTF molecules forming a dimer, $\delta_{\text{co}} \equiv \rho_{\text{rich}} - \rho_{\text{poor}} \geq 0$ is treated. The observed finite δ_{co} values in (TMTTF) $_2$ PF $_6$ below 67 K [22–24] indicate that the SP phase also has the characteristics of the CO phase of (TMTTF) $_2$ PF $_6$. In the theoretical works on other materials in terms of the PIPTs [25–28], the photoexcitations associated with the collective excitations of charges, namely, multi-excitons, have been discussed. When these concepts are applied to (TMTTF) $_2$ PF $_6$, photoexcitations of the polarization (P)-inverted domains from its ferroelectric ground state are strongly expected, which will lead to macroscopic polarization inversion, as shown in Figs. 1(a)–(c). Here, note that a dimer corresponds to a unit cell. Defining the total number of dimers as D , the bulk ferroelectric inversion is achieved when charges with $D\delta_{\text{co}}$ move from the CO ground state in the entire system.

To realize such macroscopic polarization inversion in (TMTTF) $_2$ PF $_6$, the most important

issue is to know accurately the nature of the low-energy optical excitations. For this purpose, several optical conductivities have already been observed [29–31]. However, little is known about the pure electronic excitations related to the peaks of the optical spectra. In this regard, we first observed the optical conductivity of (TMTTF)₂PF₆ at 10 K (in the SP phase) and estimated $\omega_{\text{CT}} \sim 0.128$ eV as the pure electronic excitation energy, as shown in Fig. 1(d). Details of this measurement are explained in Appendix A. A single crystal of (TMTTF)₂PF₆ was prepared by a previous method [32, 33]. The complete structure of our spectrum, as shown as a solid line in Fig. 1(d), is very similar to the previous spectra of (TMTTF)₂PF₆ at 20 K (in the CO phase) [29, 30]. This suggests that the pure electronic photoexcited state from the CO ground state can be physically considered as almost the same as that from the SP ground state. In the following sections of this article, we introduce our theoretical analyses, particularly of the optical conductivity spectrum in (TMTTF)₂PF₆, and discuss the nature of the observed peak structure exhibited as a chained line in Fig. 1(d). Throughout this paper, we consider $\hbar = e = 1$ and lattice constant = 1 for simplicity.

II. FORMULATION

Now, we consider a dimerized 1D chain model with even N_s sites, which is a quarter-filled hole system. An equal population of spins ($N_\uparrow = N_\downarrow = N_s/4$) is assumed at absolute zero temperature. Using model-specified parameters V_{eff} and V_{edge} , our Hamiltonian H is written as follows:

$$H \equiv H_t + H_{\text{Coulomb}} + V_{\text{eff}} \sum_{j:\text{even}} n_j + V_{\text{edge}} n_{N_s}, \quad (1)$$

$$H_t = - \sum_{j,\sigma} t_j \left[c_{j+1,\sigma}^\dagger c_{j,\sigma} + c_{j,\sigma}^\dagger c_{j+1,\sigma} \right], \quad (2)$$

$$H_{\text{Coulomb}} = U \sum_j n_{j,\uparrow} n_{j,\downarrow} + V \sum_j n_{j+1} n_j, \quad (3)$$

where $c_{j,\sigma}^{(\dagger)}$ denotes the annihilation (creation) operator of a hole with spin $\sigma = \uparrow, \downarrow$ at the j -th site and $n_j \equiv n_{j,\uparrow} + n_{j,\downarrow}$ represents the j -th site density operator ($n_{j,\sigma} \equiv c_{j,\sigma}^\dagger c_{j,\sigma}$). j denotes a highest occupied molecular orbital (HOMO) of a TMTTF molecule. Because each dimer has three electrons in HOMOs and the band consists of HOMOs, the system is regarded as a (third) quarter-filling in terms of holes (electrons). The dimerization of the system is treated in term t_j where $t_j \equiv t_1$ (t_2) for even (odd) j represents an inter (intra)-dimer

transfer integral. From a density functional theory (DFT) calculation of (TMTTF)₂PF₆ at 4 K [34], we select $t_1 = 0.1686$ eV and $t_2 = 0.1912$ eV. Referring to the reported Coulomb repulsive interaction strengths for (TMTTF)₂X-type compounds [15, 35], we basically use $U = 1$ eV and $V = 0.2\text{--}0.6$ eV.

Within the framework of the linear response theory, optical conductivity with respect to photon energy $\omega > 0$ and infinitesimally small positive number η is written as

$$\sigma_1(\omega) = -\frac{1}{N_s\omega} \text{Im} \left[\langle \psi_0 | J \frac{1}{\omega + i\eta + E_0 - H} J | \psi_0 \rangle \right], \quad (4)$$

where

$$J \equiv i \sum_{j,\sigma} t_j [c_{j+1,\sigma}^\dagger c_{j,\sigma} - c_{j,\sigma}^\dagger c_{j+1,\sigma}] \quad (5)$$

denotes a charge-current operator, E_0 represents the ground-state energy, and $|\psi_0\rangle$ is the ground-state wavefunction. For computational problems, $\eta/t_2 = 0.05$ (~ 0.01 eV) is used.

$\sigma_1(\omega)$ is computed by the dynamical density-matrix renormalization group (dynamical DMRG or DDMRG) scheme [36] under the open boundary condition (OBC). In general, although the numerical accuracy of a DMRG [37] calculation under the OBC is better than that under the periodic boundary condition (PBC), the charges around the edges under the OBC are rich because of breaking of the translational symmetry of the system. Although several approaches have been proposed to avoid this unphysical problem to some extent [38–40], in this study, we apply potential V_{edge} at the edge site [41] as one of its solutions and fix $V_{\text{edge}} = 50t_2$. The value of $V_{\text{edge}} = 50t_2$ is chosen as small as possible to satisfy the condition that E_0 of all the calculations hardly depend on V_{edge} due to unpermitted $V_{\text{edge}} \rightarrow +\infty$. Because the charge at the N_s -th site is poor at the V_{edge} , the CO ground state considered here has a charge-rich (poor) site at the first (N_s -th) site.

Our calculations are done with $N_s = 100$ (50 dimers). This value is enough large to satisfy with $N_s + 1 \sim N_s$ (the system size under the OBC) and to quantitatively estimate the bulk properties although finite size effects still remain in the order of $1/N_s$. The truncation number of density matrices is 400 in our all the DMRG and DDMRG calculations. All the sweep processes stopped when the numerical relative error of adjacent sweeps was less than 10^{-6} for E_0 and 10^{-3} for $\sigma_1(\omega)$.

We introduce number of photoexcited charges N_{ex} [25] to discuss the relationship between

a photoexcited state and the collective excitations of the charges. Using

$$|\psi(\omega)\rangle \equiv \frac{1}{\mathcal{N}} \frac{\eta}{(\omega + E_0 - H)^2 + \eta^2} J |\psi_0\rangle, \quad (6)$$

where \mathcal{N} denotes a normalization factor of $|\psi(\omega)\rangle$,

$$N_{\text{ex}} \equiv \sum_{j:\text{even}} [\langle \psi(\omega) | n_j | \psi(\omega) \rangle - \langle \psi_0 | n_j | \psi_0 \rangle] \quad (7)$$

can be defined. Here, $\langle \phi | n_j | \phi \rangle$ ($\phi = \psi_0, \psi(\omega)$) corresponds to the site density at the j -th site. Because we consider weak photoexcitations and a single photon injected into the system, $N_{\text{ex}} > 1$ denotes the occurrence of collective excitation. We also theoretically estimate the charge disproportion by

$$\delta_{\text{co}} \equiv \frac{1}{2} \sum_{j=49,51} |\langle \phi | n_j - n_{j+1} | \phi \rangle| \quad (0 \leq \delta_{\text{co}} \leq 1). \quad (8)$$

Because the center of the system gives most accurate expectation values of localized operators by DMRG calculations under the OBC, we choose the system centered two dimers for calculating δ_{co} .

III. RESULTS AND DISCUSSIONS FOR $V_{\text{eff}} = 0$

We first show the theoretical results for $\sigma_1(\omega)$ using several realistic values for V in the case of $V_{\text{eff}} = 0$ (the conventional model) as shown in Fig. 2(a). As it can be seen, a single peak of $\sigma_1(\omega)$ appears around the so-called dimerization gap of $\omega_{\text{d}} \equiv 2|t_1 - t_2| \sim 0.045$ eV, which corresponds to the minimum gap of free dispersions. Although this is supported by another DDMRG calculation [42] with a different parameter set [43, 44], ω_{d} deviates from ω_{CT} . In addition, in the ground state, $\delta_{\text{co}} \sim 0.03$ is the maximum value in our calculation and does not reproduce $\delta_{\text{co}} = 0.40$, which was recently observed in an X-ray diffraction experiment at 30 K [24]. To reproduce $\delta_{\text{co}} = 0.40$, we recalculate δ_{co} as a function of V by utilizing a different parameter set estimated by another DFT calculation [45], namely, $U = 2.2$ eV, $t_1 = 0.20$ eV, and $t_2 = 0.22$ eV. The results are shown in Fig. 2(b), and we determine the best parameter of $V = 0.75$ eV. However, the complete structure of $\sigma_1(\omega)$ at $V = 0.75$ eV shown in the inset of Fig. 2(b) deviates from our observation at 10 K, as shown in Fig. 1(d). In particular, the broad spectral shape significantly differs from the observed single peak, and we interpret the former feature as the exaggerated collectiveness of the

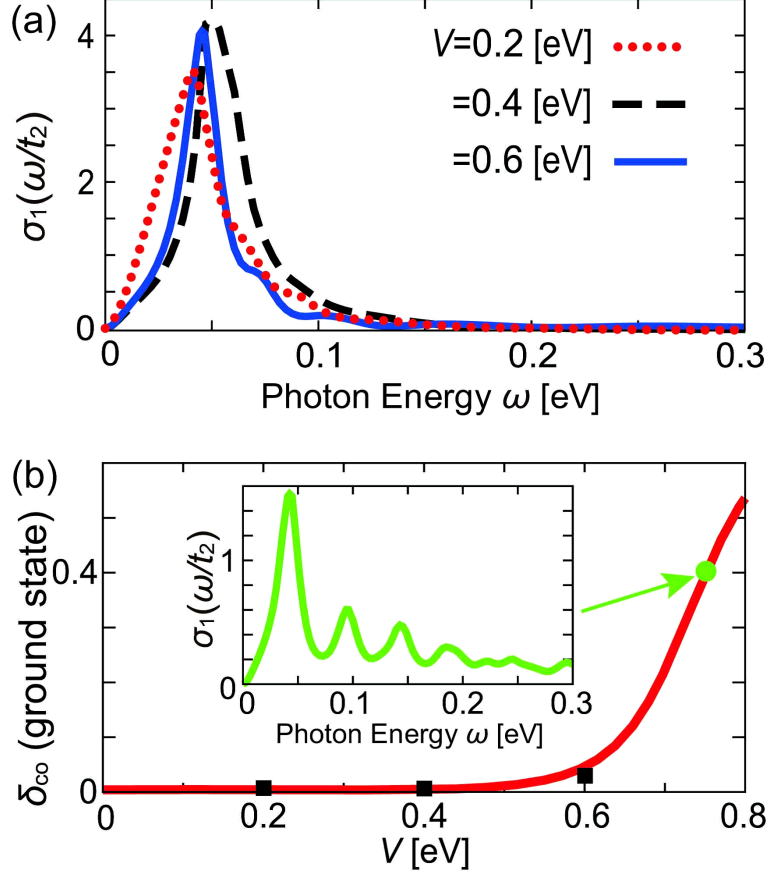


FIG. 2. DMRG and DDMRG calculations for $V_{\text{eff}} = 0$ at $N_s = 100$. (a) Results for $\sigma_1(\omega/t_2)$. (b) δ_{co} of ground states. The parameter set of $t_1 = 0.20$ eV, $t_2 = 0.22$ eV, and $U = 2.2$ eV [45] is used only for calculations presented in this figure. δ_{co} values at the ground states for the parameter sets in (a) are plotted as filled squares for comparison. The inset is $\sigma_1(\omega/t_2)$ with $t_1 = 0.20$ eV, $t_2 = 0.22$ eV, $U = 2.2$ eV [45], and $V = 0.75$ eV for giving $\delta_{\text{co}} = 0.40$ in the ground state.

excitations, which will be discussed subsequently. Thus, the conventional model ($V_{\text{eff}} = 0$) should be modified to some extent.

IV. RESULTS AND DISCUSSIONS FOR $V_{\text{eff}} \neq 0$

As an alternative approach for reproducing $\delta_{\text{co}} = 0.40$ [24], we introduce the V_{eff} term, which increases δ_{co} . Next, we employ $V/t_2 = 3.138$ ($V = 0.6$ eV) because it gives the maximum value, $\delta_{\text{co}} \sim 0.03$, in the ground state with $V_{\text{eff}} = 0$. We find $V_{\text{eff}}/t_2 = 0.086$ as the best value. The results of $\sigma_1(\omega)$ and N_{ex} with $V/t_2 = 3.138$, $V_{\text{eff}}/t_2 = 0.086$ are

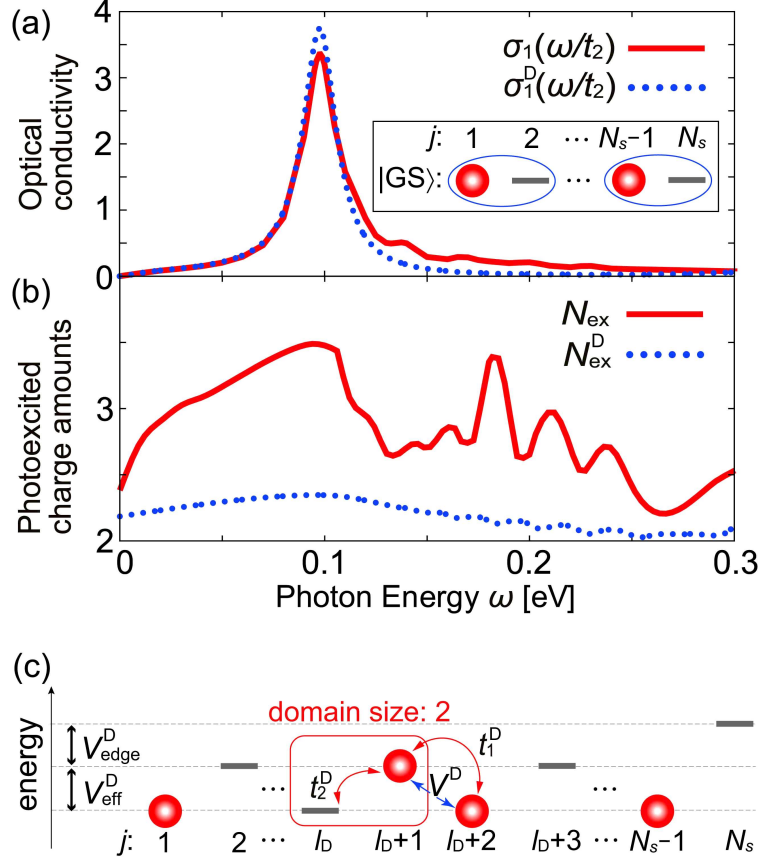


FIG. 3. Calculations of $V_{\text{eff}} \neq 0$ at $N_s = 100$. (a), (b) DDMRG results of $\sigma_1(\omega)$, N_{ex} (solid lines) and $\sigma_1^D(\omega)$, N_{ex}^D by using our effective model (dotted lines). The inset of (a) is a schematic of $|\text{GS}\rangle$ in our effective model ($\delta_{\text{co}} = 1$). The circles and horizontal bars represent single charges and empty sites, respectively. (c) Schematic energy diagram of basis $|l_D, n\rangle$ with $n = 1$ and odd l_D . Only $|l_D : \text{odd}, n\rangle$ states are generated from intra-dimer hopping.

shown in Figs. 3(a) and (b), respectively. A sharp peak structure of $\sigma_1(\omega)$ can be seen to arise around 0.10 eV, and this is clearly closer to ω_{CT} than ω_{d} . Furthermore, in Fig. 3(b), $N_{\text{ex}} \geq 2$ denotes that all the photoexcited states are the collective excitations of the charges and that maximum value $N_{\text{ex}} \sim 3.5$ appears at the sharp peak of $\sigma_1(\omega)$. As mentioned above, because $N_{\text{ex}} = \delta_{\text{co}} N_s / 2 = 20$ corresponds to the bulk ferroelectric inversion, a polarization inversion over $3.5 / \delta_{\text{co}} \sim 9$ unit cells ($3.5 / 20 \sim 18\%$ of all the charges) can be achieved at the peak. To understand this collective excitation at the peak, we compare the site density of this peak state with that of the ground state in Fig. 4(a), and we find that δ_{co} decreases to approximately 0.13. This reduction in δ_{co} at the peak can be explained by

two scenarios as follows. The photoexcited state at the peak partially includes a P-inverted domain ($\delta_{\text{co}} \rightarrow -\delta_{\text{co}} \neq 0$) or dimer–Mott (DM)-insulating state ($\delta_{\text{co}} = 0$). In this article, we discuss only the former scenario by extending the effective model proposed in Refs. [25, 26]. However, the above case of a DM-insulating state is insignificant, as discussed in Appendix B 2. In addition, we also discuss EIMV coupling [46–48] as one of the origins of unconventional term V_{eff} in Appendix B 1. V_{eff} under EIMV coupling is physically related to an effective potential representing the deformed molecular orbitals with $\delta_{\text{co}} \neq 0$.

V. EFFECTIVE MODEL ANALYSIS FOR $V_{\text{eff}} \neq 0$

Our effective model under the OBC, assumes the CO ground state obtained by the DMRG method ($\delta_{\text{co}} = 0.40$) as the charge localized limit, $\delta_{\text{co}} = 1$. The normalized ground-state wavefunction of this model, $|\text{GS}\rangle$, only contains the charges at the odd sites. Using the site density operator at the j -th site, n_j^{D} , $\langle \text{GS} | n_j^{\text{D}} | \text{GS} \rangle = 1$ (0) for odd (even) j is satisfied as approximately sketched in the inset of Fig. 3(a). All the physical parameters also differ from those of H , and in particular, U vanishes in this model. When we define basis $|l_{\text{D}}, n\rangle$ as the photoexcited state with a single P-inverted domain continuously arranged in $2n$ sites with starting site l_{D} , the Hamiltonian of our effective model is described as

$$H_{\text{dmm}} \equiv - \sum_{l_{\text{D}}, n} t(l_{\text{D}}) [|l_{\text{D}} - 2, n + 1\rangle \langle l_{\text{D}}, n| + |l_{\text{D}}, n + 1\rangle \langle l_{\text{D}}, n| + h.c.] + \sum_{l_{\text{D}}, n} E(n) |l_{\text{D}}, n\rangle \langle l_{\text{D}}, n|, \quad (9)$$

where $t(l_{\text{D}}) \equiv t_1^{\text{D}}$ (t_2^{D}) for even (odd) l_{D} and

$$E(n) = \begin{cases} nV_{\text{eff}}^{\text{D}} + V_{\text{edge}}^{\text{D}} & (l_{\text{D}} = N_s - 2n + 1) \\ V^{\text{D}} + nV_{\text{eff}}^{\text{D}} & (\text{otherwise}). \end{cases} \quad (10)$$

Here, t_1^{D} (t_2^{D}) denotes an inter (intra)-dimer transfer integral. A schematic is shown in Fig. 3(c). Eigenenergies ε_{λ} and eigenstates $|\lambda\rangle$ ($1 \leq \lambda \leq (N_s/2)^2$) satisfy $H_{\text{dmm}}|\lambda\rangle = \varepsilon_{\lambda}|\lambda\rangle \equiv \sum_{l_{\text{D}}, n} u_{\lambda}(l_{\text{D}}, n)|l_{\text{D}}, n\rangle$. Introducing the charge–current operator of this model J^{D} and $|\psi_1\rangle \equiv J^{\text{D}}|\text{GS}\rangle = i \sum_{l_{\text{D}}} (-1)^{l_{\text{D}}-1} t(l_{\text{D}}) |l_{\text{D}}, 1\rangle$, the optical conductivity of this model is defined as

$$\sigma_1^{\text{D}}(\omega) = \frac{\eta}{N_s \omega} \sum_{\lambda} \frac{|\langle \lambda | \psi_1 \rangle|^2}{(\omega - \varepsilon_{\lambda})^2 + \eta^2} \equiv \frac{\langle \psi_1 | \omega \rangle}{\mathcal{C} N_s \omega}, \quad (11)$$

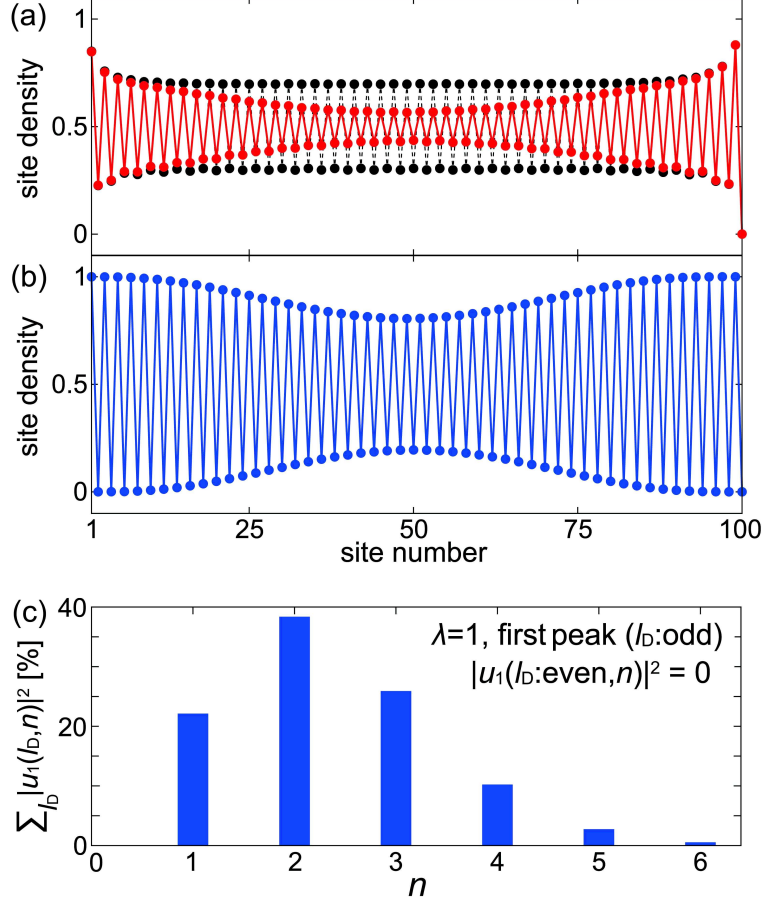


FIG. 4. Properties of the photoexcited states at the peak of both $\sigma_1(\omega)$ and $\sigma_1^D(\omega)$ with $V_{\text{eff}} \neq 0$ at $N_s = 100$. (a) Site densities of the ground state (dotted line) and peak state (solid line) by the DDMRG method. (b) Site density of the peak state by our effective model. (c) Probability weights of the peak state by our effective model with respect to basis $|l_D, n\rangle$ for odd l_D . Probability weights for even l_D are absent.

where \mathcal{C} is determined by $1 = \langle \omega | \omega \rangle$ and number of photoexcited charges

$$N_{\text{ex}}^D \equiv \sum_{j:\text{even}} [\langle \omega | n_j^D | \omega \rangle - \langle \text{GS} | n_j^D | \text{GS} \rangle] = \sum_{j:\text{even}} \langle \omega | n_j^D | \omega \rangle \quad (12)$$

can be also defined.

To relate the nature of the photoexcited state at the peak of $\sigma_1(\omega)$ to that of $\sigma_1^D(\omega)$, $\sigma_1^D(\omega)$ and N_{ex}^D should resemble $\sigma_1(\omega)$ and N_{ex} , respectively, most accurately. Employing $N_s = 100$, $t_2^D = t_2 = 0.1912$ eV, $V_{\text{edge}}^D/t_2^D = 50$, and $\eta/t_2^D = 0.05$, we succeeded in reproducing $\sigma_1(\omega)$ of $V_{\text{eff}} \neq 0$ with $t_1^D/t_2^D = 0.600$, $V^D/t_2^D = 2.615$, and $V_{\text{eff}}^D/t_2^D = 0.528$ as shown in Fig.

3(a). Although N_{ex}^{D} underestimates N_{ex} with $V_{\text{eff}} \neq 0$ as illustrated in Fig. 3(b), the overall behavior of N_{ex}^{D} is qualitatively consistent with that of N_{ex} in terms of the collective excitation of the charges ($N_{\text{ex}}^{\text{D}} > 2$) in the entire ω region. $N_{\text{ex}}^{\text{D}} \sim 2.3$ is the maximum value and appears at the peak of $\sigma_1^{\text{D}}(\omega)$. In addition, although the site density at the peak as displayed in Fig. 4(b) differs from that obtained by the DDMRG scheme in Fig. 4(a) owing to our assumption of $\delta_{\text{co}} = 1$ at the ground state, the dip structure located around the center of the system is consistent with the DDMRG result. According to the above results, the peak state of $\sigma_1(\omega)$ can be regarded as that of $\sigma_1^{\text{D}}(\omega)$, which corresponds to $\lambda = 1$ eigenstate with $\sum_{l_{\text{D}}=\text{odd}} \sum_{1 \leq n \leq 6} |u_1(l_{\text{D}} = \text{odd}, n)|^2 \sim 99.9\%$ and $u_1(l_{\text{D}} = \text{even}, n) = 0$, as shown in Fig. 4(c). This implies that the photoexcited state is generated by an intra-dimer hopping and consists of the superposition of the P-inverted domains over 1–6 unit cells.

Regarding the case of $U = 2.2$ eV mentioned already, we find much larger N_{ex} values at the peaks of the corresponding spectrum (inset of Fig. 2(b)), which are in the range 6–9. Because these large N_{ex} values indicate a strong collectiveness of the charge excitations [25], we determined that the present system lies in the category of modest collectiveness.

VI. CONCLUSIONS

To conclude, we have investigated a photoexcited state from the CO ground state of $(\text{TMTTF})_2\text{PF}_6$. We found that the calculated spectrum based on a quarter-filled 1D effective model ($V_{\text{eff}} \neq 0$) reproduce the experimental spectrum of the CO ground state. We clarified that the electronic component of the optical conductivity had a single significant peak around 0.10 eV and that the photoexcited state at the peak could be regarded as a superimposed state of the P-inverted domains with a modest collectiveness.

For the photoexcited state at the peak, approximately 18% of the charges in the system contribute to the P-inverted domains generated by a single photon (weak photoexcitation). Regarding a relative change of electric polarization ($\Delta P/P$) related to measurements of a second-harmonic generation, the photoexcitation corresponds to $\Delta P/P \sim 36\%$. The value of 36% is clearly much larger than $\Delta P/P \sim 2\text{--}10\%$ of other ferroelectric organic materials for a weak photoexcitation [7, 49]. Moreover, multi-photons (strong photoexcitation) can enhance $\Delta P/P$ and possibly generate a P-inverted domain spreading over the entire system, which is simply the achievement of bulk ferroelectric inversion. Therefore, examining strongly

photoexcited effects is one of the crucial and challenging future tasks. However, our results adequately showed that $(\text{TMTTF})_2\text{PF}_6$ could be one of promising materials for applications in optical switching devices and memories in the context of such macroscopic manipulation of ferroelectricity.

ACKNOWLEDGMENTS

This work was supported by JST CREST in Japan (Grant No. JPMJCR1661). K.I. was supported by the Grant-in-Aid for Scientific Research from JSPS in Japan (Grant No. JP17K05509). The computations were partially performed at the Research Center for Computational Science, Okazaki, Japan.

Appendix A: Details of our experiment

To evaluate the pure electronic excitation energy, we perform a fitting analysis of the optical conductivity spectrum, $\sigma(\omega)$, as shown in Fig. 1(d). It is well known that the reflectivity spectrum of a TMTTF (tetramethyltetrathiafulvalene) salt has a complex structure in the lower energy region, which is attributed to the Fano interference originating from the electron-intramolecular vibration (EIMV) coupling between the charge transfer (CT) transition and Raman active intramolecular vibration modes below 0.2 eV [31]. Fitting analyses based on the dimer model considering this effect have been performed [31, 50, 51]. In this section, we expand this method to analyze the optical spectrum.

R in Fig. A1(a) shows the reflectivity spectrum of $(\text{TMTTF})_2\text{PF}_6$ for the electric field polarized parallel to the a -axis ($E \parallel a$), which is measured by a Fourier transform infrared spectrometer. $\sigma(\omega)$ is obtained by the Kramers–Kronig transformation of the reflectivity spectrum as shown in Fig. A1(b). Considering the EIMV coupling effect in the framework of the Fano interference, we perform a fitting analysis of these spectra. The Fano interference is known to be analogous to the toy model considering classical harmonic oscillators interacting each other [52]. In this model, the vibration modes of $(\text{TMTTF})_2\text{PF}_6$ can be described as Fig. A2. The purely electronic CT transition without the EIMV coupling is regarded as an oscillator with charge q_{CT} and eigenfrequency ω_{CT} . In addition to this CT oscillator, infrared inactive intramolecular vibrations are introduced as oscillators j with

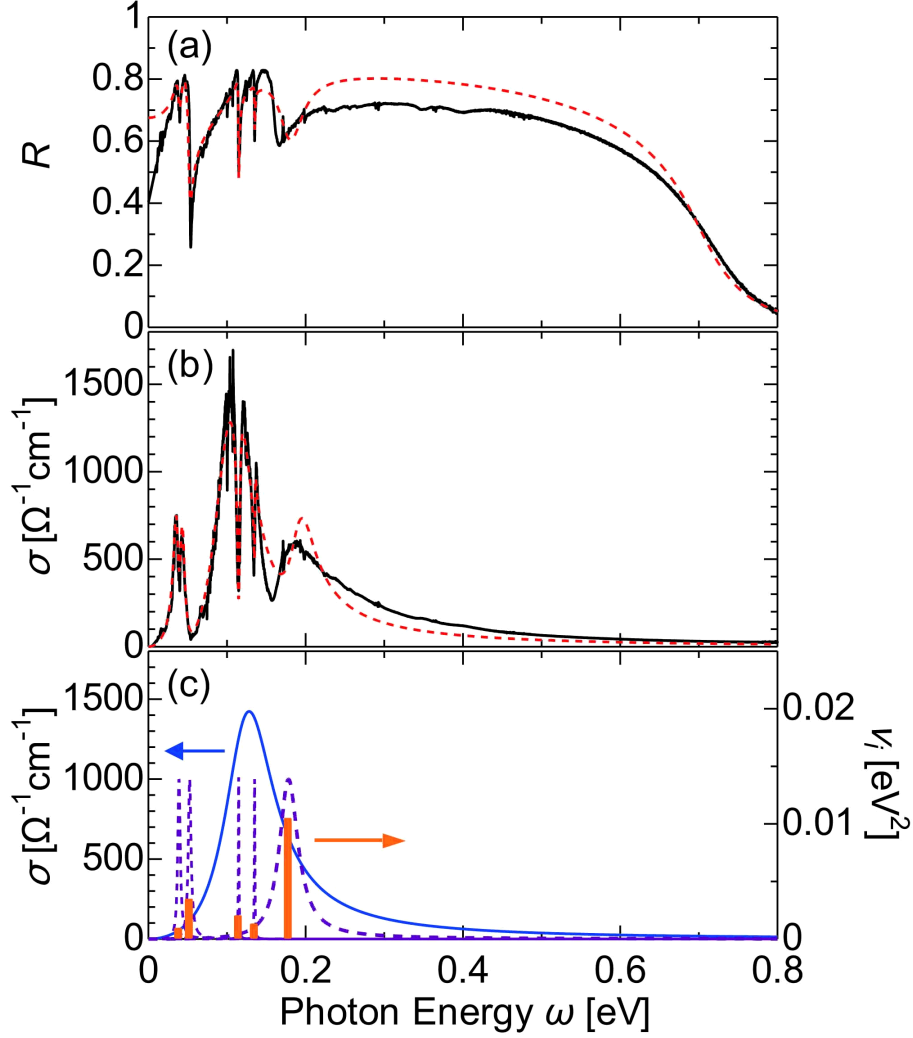


FIG. A1. (a) Polarized reflectivity and (b) optical conductivity spectrum for $E \parallel a$ at 10 K (the solid lines). The dashed lines show the fitting curves. (c) Calculated spectra of the CT transition (the solid line) and phonons (the dashed lines). The magnitude of the latter is normalized at $1000 \Omega^{-1} \text{cm}^{-1}$. The coupling between each phonon and the CT transition is shown as a bar.

eigenfrequencies ω_j ($j = 1, 2, 3, 4, 5$) without charges. Oscillator j is coupled with the CT oscillator via coupling constant ν_j . When a light having the electric field $E(t)$ is irradiated, only the CT oscillator is directly driven. Subsequently, the coupled vibration of oscillator j is generated by the vibration of the CT oscillator via the EIMV coupling. This can be attributed to the infrared activation of the original infrared inactive intramolecular vibration modes due to the interaction with the CT transition.

The equation of motion for this system with external electric field $E(\omega)$ can be expressed

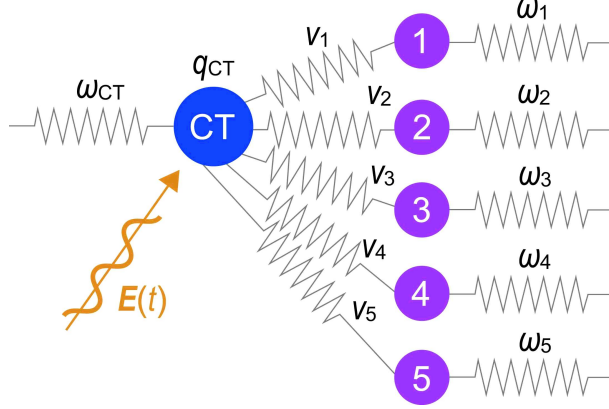


FIG. A2. Schematic of the Fano interference originating from the EIMV coupling.

as follows:

$$\begin{bmatrix} L_{\text{CT}}^{-1} & -\nu_1 & -\nu_2 & -\nu_3 & -\nu_4 & -\nu_5 \\ -\nu_1 & L_1^{-1} & 0 & 0 & 0 & 0 \\ -\nu_2 & 0 & L_2^{-1} & 0 & 0 & 0 \\ -\nu_3 & 0 & 0 & L_3^{-1} & 0 & 0 \\ -\nu_4 & 0 & 0 & 0 & L_4^{-1} & 0 \\ -\nu_5 & 0 & 0 & 0 & 0 & L_5^{-1} \end{bmatrix} \begin{bmatrix} x_{\text{CT}} \\ x_1 \\ x_2 \\ x_3 \\ x_4 \\ x_5 \end{bmatrix} = \begin{bmatrix} q_{\text{CT}} \\ 0 \\ 0 \\ 0 \\ 0 \\ 0 \end{bmatrix} E(\omega), \quad (\text{A1})$$

$$L_{\text{CT}}^{-1} = \omega_{\text{CT}}^2 - \omega^2 - i\omega\gamma_{\text{CT}}, \quad L_j^{-1} = \omega_j^2 - \omega^2 - i\omega\gamma_j,$$

where x_{CT} , x_j denote the displacements of the CT oscillator and oscillators j , respectively. From Eq. (A1),

$$x_{\text{CT}} = \frac{q_{\text{CT}}L_{\text{CT}}}{1 - L_{\text{CT}}D} E(\omega) \left(D = \sum_{j=1}^5 \nu_j^2 L_j \right) \quad (\text{A2})$$

is derived. Consequently, the dielectric function including fitting parameters can be expressed as

$$\varepsilon(\omega) = \varepsilon_{\infty} + \frac{\mu_{\text{CT}}^2 L_{\text{CT}}}{1 - L_{\text{CT}}D}. \quad (\text{A3})$$

Here, μ_{CT} is a parameter proportional to q_{CT} , corresponding to the transition intensity. ε_{∞} denotes the dielectric function of the background.

The reflectivity and optical conductivity spectra are calculated by $\varepsilon(\omega)$ in Eq. (A3). Measured reflectivity R and $\sigma(\omega)$ in Fig. A1 are well-reproduced by the fitting curves (the dashed lines). The fitting parameters are listed in Table A1. The calculated spectra of the CT transition and phonons are displayed in Fig. A1(c). From the fitting analysis,

TABLE A1. Fitting parameters in Eq. (A3)

ε_∞	ω_{CT} [eV]	γ_{CT} [eV]	μ_{CT} [eV]
1.7	0.128	7.73×10^{-2}	0.905

j	ω_j [eV]	γ_j [eV]	ν_j [eV ²]
1	0.178	2.88×10^{-2}	1.04×10^{-2}
2	0.135	9.05×10^{-4}	1.23×10^{-3}
3	0.115	9.07×10^{-4}	1.94×10^{-3}
4	0.0525	4.30×10^{-3}	3.39×10^{-3}
5	0.0389	3.79×10^{-3}	8.67×10^{-4}

the excitation energy of the pure electronic CT excitation, ω_{CT} , is evaluated to be 0.128 eV. The discrepancy between the experimental and calculated spectra in the higher energy region of $\sigma(\omega)$ is probably caused by the higher complexity of the spectral shape of the pure electronic CT transition than that of the single Lorentz oscillator assumed in this model. This is consistent with the result of our work indicating that photoexcited states are collective modes of charges.

Appendix B: Supplemental materials on theories

Before discussing the main subject of this section, we newly introduce parts of the model Hamiltonian and physical quantities. Here we consider N_s sites of a one-dimensional (1D) chain model with a quarter-filled hole system and an equal population of spins ($N_\uparrow = N_\downarrow = N_s/4$) at absolute zero temperature again. In addition to Eqs. (1)–(3), we newly define parts of the model Hamiltonian as follows:

$$H_{\text{eff}}^{\text{even}} = V_{\text{eff}} \sum_{j:\text{even}} n_j, \quad H_{\text{eff}}^{\text{odd}} = V_{\text{eff}} \sum_{j:\text{odd}} n_j. \quad (\text{B1})$$

In this section, Hamiltonian $H_t + H_{\text{Coulomb}} + H_{\text{eff}}^{\text{even}}$ is the same as H in Eq. (1) with $V_{\text{edge}} = 0$. Using given Hamiltonian \mathcal{H} and the charge-current operator J in Eq. (5), the reduced optical

conductivity of given photon energy $\omega > 0$ is written as

$$\sigma_{\text{IR}}(\omega) = -\frac{1}{N_s} \text{Im} \left[\langle \psi_0 | J \frac{1}{\omega + i\eta + E_0 - \mathcal{H}} J | \psi_0 \rangle \right] \quad (\text{B2})$$

within the framework of the linear response theory for $\eta \rightarrow 0+$. Parameters with $V_{\text{eff}} \neq 0$ in previous sections (namely, $t_1/t_2 = 0.882$, $U/t_2 = 5.230$, $V/t_2 = 3.138$, and $\eta/t_2 = 0.05$ for $t_2 = 0.1912$ eV [15, 34, 35]) are utilized for all the computations in this section.

In this section, all the calculations are performed by the exact diagonalization (ED) method under the periodic boundary condition (PBC) to avoid the edge effects that typically occur under the open boundary condition (OBC). Because the ED calculations are limited to a small system size of the order of $N_s \sim 20$ for the computational problem, the edge effects significantly affect the calculations and so, should be eliminated. In contrast to the density-matrix renormalization group (DMRG) [37] and dynamical DMRG (DDMRG) [36] methods in previous sections, the ED method for a fixed system size can easily yield the wavefunctions of arbitrary quantum states and allow their comparison owing to the unused renormalized Hamiltonians even if the calculations involve different physical parameters. This is the reason why we select the ED method in this section.

1. Estimation of V_{eff}

The aim of this subsection is to discuss one of the origins of $V_{\text{eff}} = 0.086t_2$ in previous sections. As mentioned already, an unconventional term, V_{eff} , is introduced for reproducing the experimental data and indeed consider several origins of V_{eff} such as the quasi-two-dimensional effects from the Coulomb interactions between 1D chains. However, we consider that one of the candidates for the origin of V_{eff} is the electron-intramolecular vibration (EIMV) coupling, which is one of the effective electron-phonon coupling models [46–48]. Using Eqs. (2) and (3), our starting Hamiltonian, H_{eph} , is written as

$$H_{\text{eph}} \equiv H_t + H_{\text{Coulomb}} + H_{\text{EIMV}}, \quad (\text{B3})$$

$$H_{\text{EIMV}} = - \sum_{\alpha,j} S_\alpha x_j^\alpha n_j + \sum_{\alpha,j} \frac{S_\alpha}{2} (x_j^\alpha)^2, \quad (\text{B4})$$

where x_j^α denotes the dimensionless reference frame of molecular vibration mode α at the j -th site. For a certain vibration mode, α , we represent g_α as an EIMV coupling constant and Ω_α as a frequency of a molecular vibration, respectively. Then $S_\alpha = 2g_\alpha^2/\Omega_\alpha$. Here,

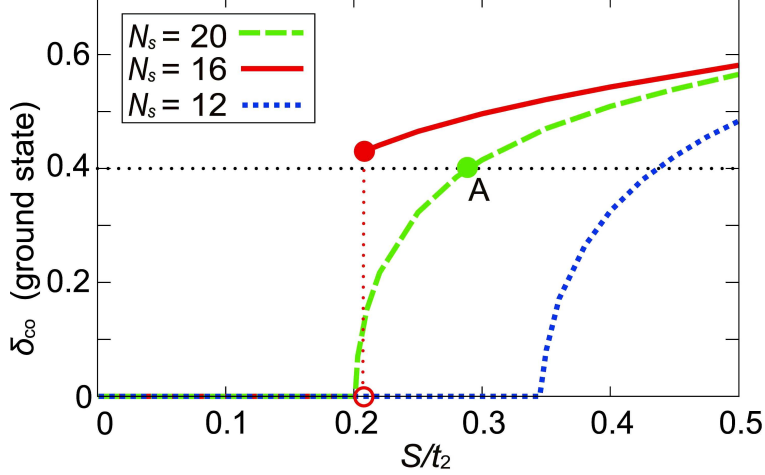


FIG. B1. Calculations of δ_{co} for S/t_2 determined by minimizing E_0^{EIMV} in Eq. (B8) for $N_s = 12, 16, 20$ with the ED method under the PBC. The horizontal dotted-line and point A correspond to $\delta_{\text{co}} = 0.40$ [24].

we introduce the mean fields of charge disproportion δ_{co} and amplitude of the molecular vibration x_0^α as follows.

$$\langle \psi_0 | n_j | \psi_0 \rangle = \frac{1}{2} + (-1)^{j-1} \frac{\delta_{\text{co}}}{2}, \quad (\text{B5})$$

$$x_j^\alpha = (-1)^{j-1} x_0^\alpha. \quad (\text{B6})$$

After considering the appropriate constant energy shift and comparing H_{eph} in Eq. (B3) with $H_t + H_{\text{Coulomb}} + H_{\text{eff}}^{\text{even}}$ (see Eqs. (2), (3), and (B1)), which is the same as H in Eq. (1) with $V_{\text{edge}} = 0$,

$$V_{\text{eff}} = \sum_{\alpha} S_{\alpha} \delta_{\text{co}} \quad (\text{B7})$$

is derived by the Hellmann–Feynman theorem. In the charge-ordered (CO) ground state, because a finite δ_{co} deforms the molecular orbitals associated with n_j for each site, V_{eff} in Eq. (B7) can be interpreted as an effective potential representing such deformation.

To simplify the problem, we select a single molecular vibration mode, β ($S_{\alpha} = 0, x_j^{\alpha} = 0$ for $\alpha \neq \beta$), and define $S_{\beta} \equiv S, x_j^{\beta} \equiv x_0$. Then, we can derive $x_0 = \delta_{\text{co}}/2$ similarly to as discussed above. δ_{co} for a fixed S/t_2 is determined by minimizing ground-state energy E_0^{EIMV} written as

$$E_0^{\text{EIMV}} = \langle \psi_0 | H_{\text{eph}} | \psi_0 \rangle \quad (x_0 = \delta_{\text{co}}/2). \quad (\text{B8})$$

Within the framework of the ED calculation under the PBC, the results of δ_{co} for $N_s = 12, 16, 20$ are shown in Fig. B1. To avoid the finite size effect, we use the result for $N_s = 20$, which is the largest system size in our calculations, and estimate V_{eff} .

In a recent experiment [24], because $\delta_{\text{co}} = 0.40$ was observed in the CO ground state at 30 K, $V_{\text{eff}} = S\delta_{\text{co}} \sim 0.116t_2 \equiv V_{\text{eff}}^{\text{ED}}$ could be estimated at $\delta_{\text{co}} = 0.40$ by using value $S/t_2 = 0.291$ for $N_s = 20$ at point A, as shown in Fig. B1. The estimated value of $V_{\text{eff}}^{\text{ED}}$ is close to $V_{\text{eff}} = 0.086t_2$.

Apart from the structural similarity to the first-order phase transition seen in Fig. B1, value S/t_2 vanishes with δ_{co} of $N_s = 16$ and $N_s = 20$ is quantitatively regarded as practically unchanged. Therefore, our ED calculations presented in the next subsection, focus on $N_s = 16$.

Here, we briefly comment on the origin of the first-order phase transition noted in Fig. B1. According to the observed T - P phase diagram of $(\text{TMTTF})_2\text{PF}_6$ [9], the spin-Peierls (SP) phase should be the ground state at $T = 0$ and, in general, it should have both $4k_{\text{F}}$ -charge density wave (CDW) and $2k_{\text{F}}$ -spin density wave (SDW) instabilities [53], where k_{F} denotes a Fermi wave number. In this subsection, we only set CO mean field δ_{co} that has a $4k_{\text{F}}$ instability and do not treat the $2k_{\text{F}}$ instability of an antiferromagnetic order appearing in the SP state. Consequently, a tetrameric model should be considered for ensuring the second-order phase transition of δ_{co} , which is our future work.

2. Dimer–Mott state in the excited state

In this subsection, we investigate the relationship between the dimer–Mott (DM) state and the photoexcited state by means of the ED method under the PBC. All the calculations are conducted at $N_s = 16$ as discussed in the previous subsection. In addition, we also inquire regarding the existence of the polarization (P)-inverted CO state in the photoexcited state for comparison. For this purpose, using Eqs. (2), (3), and (B1), we introduce three Hamiltonians defined as

$$H_1 \equiv H_t + H_{\text{Coulomb}} + H_{\text{eff}}^{\text{even}}, \quad (\text{B9})$$

$$H_2 \equiv H_t + H_{\text{Coulomb}} + H_{\text{eff}}^{\text{odd}}, \quad (\text{B10})$$

$$H_3 \equiv H_t + H_{\text{Coulomb}}(V = 0). \quad (\text{B11})$$

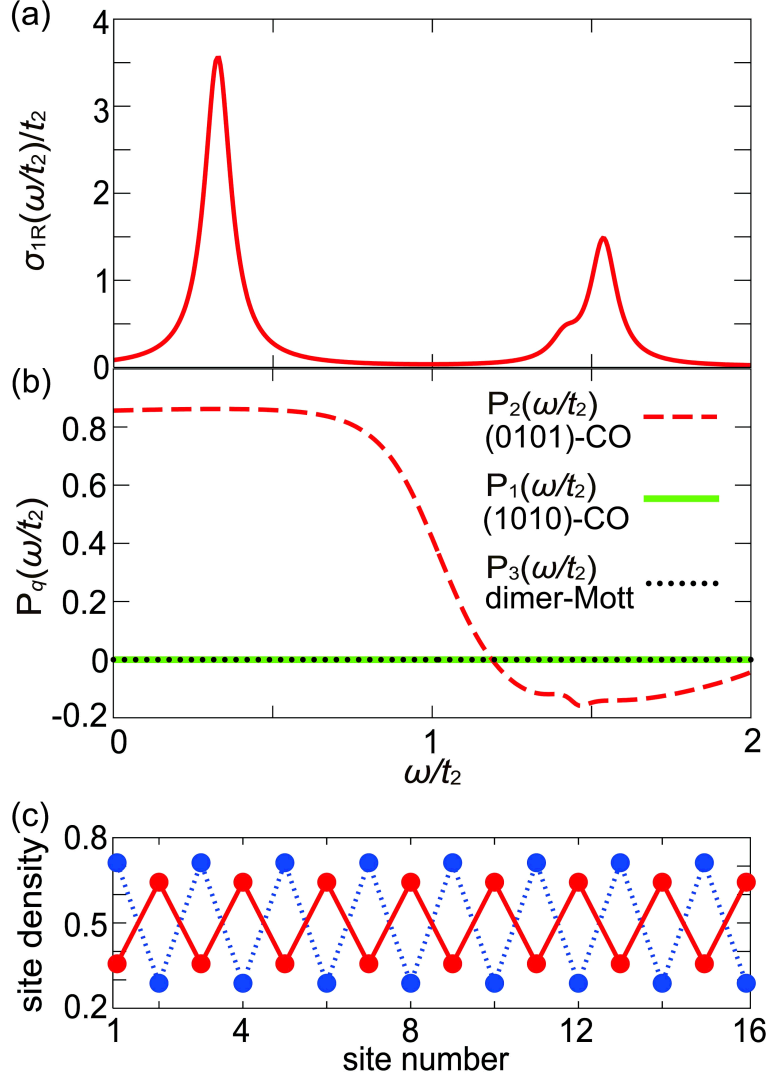


FIG. B2. Calculations by the ED method under the PBC for $N_s = 16, \eta/t_2 = 0.05$. (a) Computed $\sigma_{1R}(\omega/t_2)$ of H_1 in Eq. (B9). (b) Projections of a state, $|\Phi_1(\omega)\rangle$, onto the ground states at different physical phases $|\Psi_1\rangle$ ((1010)-CO), $|\Psi_2\rangle$ ((0101)-CO), and $|\Psi_3\rangle$ (dimer-Mott). (c) Site densities. The solid line connected with solid circles describes the site density of the photoexcited state at the first peak of $\sigma_{1R}(\omega/t_2)$ shown in (a). For comparison, the site density of the ground state is displayed as a dotted line with filled circles.

From the discussions in previous sections, because H_1 in Eq. (B9) corresponds to original Hamiltonian H with $V_{\text{edge}} = 0$ in Eq. (1), the ground state of H_1 in Eq. (B9) defined as $|\Psi_1\rangle$ is rich in charges on every odd site and we symbolically represent this as “(1010)-CO.” In contrast, defining $|\Psi_2\rangle$ as the ground state of H_2 in Eq. (B10) and $|\Psi_2\rangle$ as having rich

charges on each even site, which we symbolically represent as “(0101)-CO.” This state can be ascribed as a P-inverted CO state with respect to $|\Psi_1\rangle$. The DM ground state, $|\Psi_3\rangle$, considers the ground state of H_3 in Eq. (B11), and we simply refer $|\Psi_3\rangle$ as a “dimer–Mott.” Although some theoretical works have revealed the phase diagram of the ground state in 1D quarter-filled Hamiltonian $H_t + H_{\text{Coulomb}}$ (see Eqs. (2) and (3)) and the parameter region of the DM phase with non-vanishing U and V [15, 35], we particularly choose $V = 0$ in H_3 (Eq. (B11)) for completely neglecting the charge-ordering effects originating from $V \neq 0$.

We calculate a photoexcited state with given photon energy ω and J in Eq. (5) as

$$|\Phi_1(\omega)\rangle \equiv \frac{1}{\mathcal{N}_1} \frac{\eta}{(\omega - E_1 + H_1)^2 + \eta^2} J |\Psi_1\rangle, \quad (\text{B12})$$

where E_1 represents the ground-state energy of H_1 in Eq. (B9). \mathcal{N}_1 is determined by satisfying $1 = \langle \Phi_1(\omega) | \Phi_1(\omega) \rangle$. In addition to this, we also calculate

$$P_q(\omega) \equiv \langle \Psi_q | \Phi_1(\omega) \rangle \quad (q = 1, 2, 3) \quad (\text{B13})$$

which denotes the characteristic quantities for qualitatively estimating the mixing degrees of the different ground states $|\Psi_{q=1,2,3}\rangle$ with respect to $|\Phi_1(\omega)\rangle$.

$\sigma_{\text{IR}}(\omega/t_2)$ with $\mathcal{H} = H_1$, $E_0 = E_1$, and $|\psi_0\rangle = |\Psi_1\rangle$ in Eq. (B2) is shown in Fig. B2(a). Our calculations of $P_{q=1,2,3}(\omega)$ are displayed in Fig. B2(b). $V_{\text{eff}}/t_2 = 0.086$ is chosen for the calculations presented here. This values also allow discussing the same photoexcitation calculated under the OBC in the previous sections except for finite size effects. As it can be seen, in addition to the obvious result of $P_1(\omega) = 0$, it is clear that $P_2(\omega) \neq 0$ and $P_3(\omega) = 0$. In particular, $P_2(\omega) \sim 1$ can be seen around the first peak of $\sigma_{\text{IR}}(\omega/t_2)$. Therefore, the photoexcited state at the first peak is highly inclusive of the P-inverted state, $|\Psi_2\rangle$ ((0101)-CO), regarding the $|\Psi_1\rangle$ ((1010)-CO) ground state, but it is exclusive of the DM state, $|\Psi_3\rangle$. Compared to the site density of the ground state $\langle \Psi_1 | n_j | \Psi_1 \rangle$, the enhancement of the “(0101)-CO” photoexcited state at the first peak is consistent with site density at the peak $\langle \Phi_1(\omega) | n_j | \Phi_1(\omega) \rangle$ shown in Fig. B2(c).

[1] H. Okamoto, *Ultrafast photoinduced phase transitions in one-dimensional organic correlated electron systems*, Molecular Electronic and Related Materials-Control and Probe with Light, 59-97, Transworld Research Network (2010).

- [2] D. N. Basov, R. D. Averitt, D. van der Marel, M. Dressel, and K. Haule, *Rev. Mod. Phys.* **83**, 471 (2011).
- [3] S. Iwai, K. Yamamoto, A. Kashiwazaki, F. Hiramatsu, H. Nakaya, Y. Kawakami, K. Yakushi, H. Okamoto, H. Mori, and Y. Nishio, *Phys. Rev. Lett.* **98**, 097402 (2007).
- [4] K. Yamamoto, S. Iwai, S. Boyko, A. Kashiwazaki, F. Hiramatsu, C. Okabe, N. Nishi, and K. Yakushi, *J. Phys. Soc. Jpn.* **77**, 074709 (2008).
- [5] H. Yamakawa, T. Miyamoto, T. Morimoto, H. Yada, Y. Kinoshita, M. Sotome, N. Kida, K. Yamamoto, K. Iwano, Y. Matsumoto, S. Watanabe, Y. Shimoi, M. Suda, H. M. Yamamoto, H. Mori, and H. Okamoto, *Sci. Rep.* **6**, 20571 (2016).
- [6] T. Luty, H. Cailleau, S. Koshihara, E. Collet, M. Takesada, M. H. L.-Cailleau, M. B.-Le Cointe, N. Nagaosa, Y. Tokura, E. Zienkiewicz, and B. Ouladdiaf, *Europhys. Lett.* **59**, 619 (2002).
- [7] K. Iwano, Y. Shimoi, T. Miyamoto, D. Hata, M. Sotome, N. Kida, S. Horiuchi, and H. Okamoto, *Phys. Rev. Lett.* **118**, 107404 (2017).
- [8] B. Salameh, S. Yasin, M. Dumm, G. Untereiner, L. Montgomery, and M. Dressel, *Phys. Rev. B* **83**, 205126 (2011).
- [9] B. Köhler, E. Rose, M. Dumm, G. Untereiner, and M. Dressel, *Phys. Rev. B* **84**, 035124 (2011).
- [10] K. Medjanik, M. de Souza, D. Kutnyakhov, A. Gloskovskii, J. Müller, M. Lang, J.-P. Pouget, P. F.-Leylekian, A. Moradpour, H.-J. Elmers, and G. Schönense, *Eur. Phys. J. B* **87**, 256 (2014).
- [11] S. Tomić and M. Dressel, *Rep. Prog. Phys.* **78**, 096501 (2015).
- [12] I. Voloshenko, M. Herter, R. Beyer, A. Pustogow, and M. Dressel, *J. Phys.: Condens. Matter* **29**, 115601 (2017).
- [13] H. Wilhelm, D. Jaccard, R. Duprat, C. Bourbonnais, D. Jérôme, J. Moser, C. Carcel, and J. M. Fabre, *Eur. Phys. J. B* **21**, 175 (2001).
- [14] L. Degiorgi and D. Jérôme, *J. Phys. Soc. Jpn.* **75**, 051004 (2006).
- [15] H. Seo, J. Merino, H. Yoshioka, and M. Ogata, *J. Phys. Soc. Jpn.* **75**, 051009 (2006).
- [16] F. Iwase, K. Sugiura, K. Furukawa, and T. Nakamura, *J. Phys. Soc. Jpn.* **78**, 104717 (2009).
- [17] H. Seo and H. Fukuyama, *J. Phys. Soc. Jpn.* **66**, 1249 (1997).
- [18] D. S. Chow, F. Zamborszky, B. Alavi, D. J. Tantillo, A. Baur, C. A. Merlic, and S. E. Brown,

- Phys. Rev. Lett. **85**, 1698 (2000).
- [19] P. Monceau, F. Y. Nad, and S. Brazovskii, Phys. Rev. Lett. **86**, 4080 (2001).
- [20] M. Dressel, M. Dumm, T. Knoblauch, and M. Masino, Crystals **2**, 528 (2012).
- [21] M. de Souza, L. Squillante, C. Sônego, P. Menegasso, P. Foury-Leylekian, and J.P. Pouget, Phys. Rev. B **97**, 045122 (2018).
- [22] A. Pustogow, T. Peterseim, S. Kolatschek, L. Engel, and M. Dressel, Phys. Rev. B **94**, 195125 (2016).
- [23] R. Świetlik, B. Barszcz, A. Pustogow, and M. Dressel, Phys. Rev. B **95**, 085205 (2017).
- [24] S. Kitou, T. Fujii, T. Kawamoto, N. Katayama, S. Maki, E. Nishibori, K. Sugimoto, M. Takata, T. Nakamura, and H. Sawa, Phys. Rev. Lett. **119**, 065701 (2017).
- [25] K. Iwano, Phys. Rev. Lett. **97**, 226404 (2006); Phys. Rev. Lett. **102**, 106405 (2009); Phys. Rev. B **91**, 115108 (2015).
- [26] M. Mayr and P. Horsch, Phys. Rev. B **73**, 195103 (2006).
- [27] K. Onda, S. Ogihara, K. Yonemitsu, N. Maeshima, T. Ishikawa, Y. Okimoto, X. Shao, Y. Nakano, H. Yamochi, G. Saito, and S.Y. Koshihara, Phys. Rev. Lett. **101**, 067403 (2008).
- [28] H. Hashimoto, H. Matsueda, H. Seo, and S. Ishihara, J. Phys. Soc. of Jpn. **83**, 123703 (2014).
- [29] V. Vescoli, L. Degiorgi, W. Henderson, G. Grüner, K. P. Starkey, and L. K. Montgomery, Science **281**, 1181 (1998).
- [30] M. Dumm, M. Abaker, M. Dressel, and L. K. Montgomery, J. Low Temp. Phys. **142**, 613 (2006).
- [31] Y. Naitoh, Y. Kawakami, T. Ishikawa, Y. Sagae, H. Itoh, K. Yamamoto, T. Sasaki, M. Dressel, S. Ishihara, Y. Tanaka, K. Yonemitsu, and S. Iwai, Phys. Rev. B **93**, 165126 (2016).
- [32] T. Nakamura, J. Phys. Soc. Jpn. **72**, 213 (2003).
- [33] T. Nakamura, K. Furukawa, and T. Hara, J. Phys. Soc. Jpn. **76**, 064715 (2007).
- [34] A. C. Jacko, H. Feldner, E. Rose, F. Lissner, M. Dressel, R. Valentí, and H. O. Jeschke, Phys. Rev. B **87**, 155139 (2013).
- [35] M. Tsuchiizu, H. Yoshioka, and Y. Suzumura, J. Phys. Soc. Jpn. **68**, 1809 (1999); J. Phys. Soc. Jpn. **70**, 1460 (2001).
- [36] E. Jeckelmann, Phys. Rev. B **66**, 045114 (2002).
- [37] S. R. White, Phys. Rev. Lett. **69**, 2863 (1992); Phys. Rev. B **48**, 10345 (1993).
- [38] M. Vekić and S. R. White, Phys. Rev. Lett. **71**, 4283 (1993).

- [39] A. Gendiar, R. Krcmar, and T. Nishino, *Prog. Theo. Phys.* **122**, 953 (2009).
- [40] N. Shibata and C. Hotta, *Phys. Rev. B* **84**, 115116 (2011).
- [41] S. R. White and D. A. Huse, *Phys. Rev. B* **48**, 3844 (1993).
- [42] H. Benthien and E. Jeckelmann, *Eur. Phys. J. B* **44**, 287 (2005).
- [43] F. Mila, *Phys. Rev. B* **52**, 4788 (1995).
- [44] L. Ducasse, M. Abderrabbat, J. Hoaraut, M. Pesquert, B. Gallois, and J. Gaultier, *J. Phys. C: Solid State Phys.* **19**, 3805 (1986).
- [45] G. Giovannetti, S. Kumar, J.-P. Pouget, and M. Capone, *Phys. Rev. B* **85**, 205146 (2012).
- [46] M. J. Rice, *Solid State Communications* **31**, 93 (1979).
- [47] K. Nasu, *J. Phys. Soc. Jpn.* **53**, 302 (1984).
- [48] A. Painelli and A. Girlando, *J. Chem. Phys.* **84**, 5655 (1986).
- [49] T. Umanodan, S. Tanaka, S. Naruse, T. Ishikawa, K. Onda, S. Koshihara, S. Horiuchi, and Y. Okimoto, *J. Phys. Soc. Jpn.* **84**, 073707 (2015).
- [50] M. J. Rice, V. M. Yartsev, and C. S. Jacobsen, *Phys. Rev. B* **21**, 3437 (1980).
- [51] C. S. Jacobsen, D. B. Tanner, and K. Bechgaard, *Phys. Rev. B* **28**, 7019 (1983).
- [52] Y. S. Joe, A. M. Satanin, and C. S. Kim, *Phys. Scr.* **74**, 259 (2006).
- [53] J. E. Hirsch and D. J. Scalapino, *Phys. Rev. Lett.* **50**, 1168 (1983); *Phys. Rev. B* **27**, 7169 (1983); *Phys. Rev. B* **29**, 5554 (1984).